International Journal of Solids and Structures 60–61 (2015) 66–74

Contents lists available at ScienceDirect

International Journal of Solids and Structures

journal homepage: www.elsevier.com/locate/ijsolstr

Static deformation of a spherically anisotropic and multilayered magneto-electro-elastic hollow sphere

J.Y. Chen [a], E. Pan [b,*], P.R. Heyliger [c]

[a] School of Mechanical Engineering, Zhengzhou University, Zhengzhou 450001, PR China
[b] Department of Civil Engineering, University of Akron, OH 44325, USA
[c] Department of Civil and Environmental Engineering, Colorado State University, CO 80523, USA

ARTICLE INFO

Article history:
Received 2 December 2014
Received in revised form 3 February 2015
Available online 13 February 2015

Keywords:
Spherical system of vector functions
Propagation matrix method
Multiferroics composite
Multilayered MEE sphere

ABSTRACT

In this paper, we present an analytical solution on the general static deformation of a spherically anisotropic and multilayered magneto-electro-elastic (MEE) hollow sphere. We first express the general solution in each layer in terms of the spherical system of vector functions where two transformations of variables are also proposed to achieve the analytical results. The spherical system of vector functions can be applied to expand any vector as well as scalar function, and it further automatically separates the static deformation into two independent sub-problems: The LM-type and N-type. The LM-type is associated with the spheroidal deformation and is coupled further with the electric and magnetic fields. The N-type is associated with the torsional deformation and is purely elastic and independent of the electric and magnetic fields. To solve the multilayered spherical problem, the propagation matrix method is introduced with the propagation matrix being simply the exponential matrix for each layer. By assuming the continuity conditions on the interface between the adjacent spherical shells, the solution can be simply propagated from the inner surface to the outer surface of the layered and hollow MEE sphere so that specific boundary value problems can be solved. As numerical examples, a three-layered sandwich hollow sphere with different stacking sequences under different boundary conditions is studied. Our results illustrate the influence of the stacking sequences while showing the effectiveness of the proposed method.

1. Introduction

Magneto-electro-elastic (MEE) materials and structures attract many researchers because of their excellent ability of converting energy among the electric, mechanical, and magnetic fields. As such, they have huge potential applications in smart sensors, actuators, filters among others, as reviewed in material community as multiferroics and multiferroic composites (Eerenstein et al., 2006; Nan et al., 2008).

In the past two decades, studies of these solids were concentrated primarily on MEE layered plates under both static and dynamic deformation. Pan (2001) and Wang and co-workers (2003) analyzed multilayered MEE rectangular plates under static loadings with the propagation matrix method. In constructing the propagation matrix, they employed the Stroh formalism and the state-space method. Pan and Heyliger (2002) and Chen and co-workers (2007a) investigated the corresponding free vibration problem in the layered rectangular and multilayered MEE plates. The dispersion relation of wave propagation in multilayered MEE plates with infinite dimensions in the horizontal plane was derived and analyzed by Chen and co-workers (2007b) and Yu and co-workers (2012). More recent studies include guided waves in layered MEE bars with rectangular cross-sections (Yu et al., 2014) and free vibrations in layered plates under more complicated lateral boundary conditions (Chen et al., 2014).

Compared to the horizontally layered structure, a layered sphere poses more of a challenge. Ding and Chen (1996) calculated the natural frequencies of an elastic spherically isotropic hollow sphere submerged in a compressible fluid medium. Based on the state-space method and variables separation techniques, Chen and Ding (2001) and Chen and co-workers (2001) investigated, respectively, the free vibration of hollow elastic sphere and the static deformation of multilayered piezoelectric hollow spheres. Heyliger and Wu (1999) derived an analytical solution for the radial deformation of a layered piezoelectric sphere. However, to the best of the authors' knowledge, the general static deformation of a multilayered MEE hollow sphere with spherical anisotropy has

* Corresponding author. Tel.: +1 330 972 6739 (O); fax: +1 330 972 6020.
E-mail address: pan2@uakron.edu (E. Pan).

http://dx.doi.org/10.1016/j.ijsolstr.2015.02.004
0020-7683/

not been analyzed so far. Furthermore, our recent studies indicate that a spherical and layered shell structure could be more efficient and powerful than a cylindrical and layered shell in terms of the produced coupling effect between the magnetic and electric fields (under preparation). This absence motivates the present study.

This paper is organized as follows: After the introduction, in Section 2, we describe the problem to be solved and present the basic equations in spherical coordinates for the spherically anisotropic MEE material. In Section 3, we introduce the spherical system of vector functions along with its properties. In Section 4, the general solutions in the analytical form for each layer and the propagation matrix in terms of the exponential matrix are derived. Numerical examples are presented in Section 5 and conclusions are drawn in Section 6.

2. Problem description and basic equations

We assume, as shown in Fig. 1, a spherically anisotropic and p-layered MEE hollow sphere. The ith layer has a radius of r_i on its interior interface and r_{i+1} on its exterior interface. Thus, the inner and outer surface of the layered sphere has, respectively, a radius of r_1 and r_{p+1}, and is under suitable boundary conditions which will be presented later. The interface between the adjacent layers is assumed to be perfectly connected. In other words the extended displacements and tractions in r-direction are continuous. Spherical anisotropy means that in the spherical coordinates (r, θ, ϕ), the center of the spherical isotropy is coincident with the origin and the symmetry axis of the material is along r-direction. We further mention that only under this assumption of spherical anisotropy, we can derive the analytical solutions as presented in this paper; the general anisotropic case has to be solved numerically.

For this general problem, the following equations must be satisfied at every point inside each of the individual layers in terms of the spherical coordinates. The general constitutive relations of the MEE structure with spherical anisotropy are given as follows:

$$
\begin{aligned}
&\sigma_{\theta\theta}=c_{11}\gamma_{\theta\theta}+c_{12}\gamma_{\varphi\varphi}+c_{13}\gamma_{rr}-e_{31}E_r-q_{31}H_r;\quad \sigma_{r\theta}=2c_{44}\gamma_{r\theta}-e_{15}E_\theta-q_{15}H_\theta\\
&\sigma_{\varphi\varphi}=c_{12}\gamma_{\theta\theta}+c_{11}\gamma_{\varphi\varphi}+c_{13}\gamma_{rr}-e_{31}E_r-q_{31}H_r;\quad \sigma_{r\varphi}=2c_{44}\gamma_{r\varphi}-e_{15}E_\varphi-q_{15}H_\varphi\\
&\sigma_{rr}=c_{13}\gamma_{\theta\theta}+c_{13}\gamma_{\varphi\varphi}+c_{33}\gamma_{rr}-e_{33}E_r-q_{33}H_r;\quad \sigma_{\theta\varphi}=2c_{66}\gamma_{\theta\varphi}\\
&D_\theta=2e_{15}\gamma_{\theta r}+\varepsilon_{11}E_\theta+\alpha_{11}H_\theta;\quad D_\varphi=2e_{15}\gamma_{\varphi r}+\varepsilon_{11}E_\varphi+\alpha_{11}H_\varphi\\
&D_r=e_{31}(\gamma_{\theta\theta}+\gamma_{\varphi\varphi})+e_{33}\gamma_{rr}+\varepsilon_{33}E_r+\alpha_{33}H_r\\
&B_\theta=2q_{15}\gamma_{\theta r}+\alpha_{11}E_\theta+\mu_{11}H_\theta;\quad B_\varphi=2q_{15}\gamma_{\varphi r}+\alpha_{11}E_\varphi+\mu_{11}H_\varphi\\
&B_r=q_{31}(\gamma_{\theta\theta}+\gamma_{\varphi\varphi})+q_{33}\gamma_{rr}+\alpha_{33}E_r+\mu_{33}H_r
\end{aligned}
\tag{1}
$$

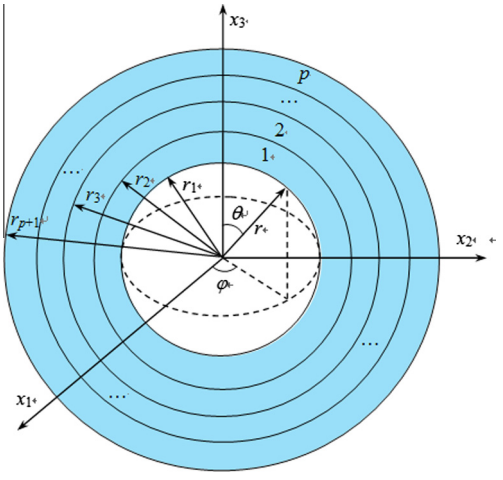

Fig. 1. A hollow MEE sphere made of p layers with its inner surface at r_1 and outer surface at r_{p+1}. Both surfaces are subjected to suitable extended displacement and traction boundary conditions.

where σ_{ij}, D_i and B_i are the stress, electric displacement and magnetic induction, respectively; γ_{ij}, E_i and H_i are the strain, electric field and magnetic field, respectively; c_{ik}, ε_{ik} and μ_{ik} are the elastic, dielectric, and magnetic permeability coefficients, respectively; e_{ik} and q_{ik} are the piezoelectric and piezomagnetic coefficients, respectively; α_{ij} are the electromagnetic coefficients. It is noted that an additional relationship $c_{11}=c_{12}+2c_{66}$ holds for the spherically anisotropic material with the r-axis being the axis of symmetry.

In Eq. (1), the strains, electric and magnetic fields are related to the elastic displacement and electric and magnetic potentials by

$$
\begin{aligned}
&\gamma_{rr}=\frac{\partial u_r}{\partial r};\quad \gamma_{\theta\theta}=\frac{1}{r}\frac{\partial u_\theta}{\partial\theta}+\frac{u_r}{r};\quad \gamma_{\varphi\varphi}=\frac{1}{r\sin\theta}\frac{\partial u_\varphi}{\partial\varphi}+\frac{u_\theta}{r}\cot\theta+\frac{u_r}{r}\\
&2\gamma_{r\theta}=\frac{\partial u_\theta}{\partial r}-\frac{u_\theta}{r}+\frac{1}{r}\frac{\partial u_r}{\partial\theta};\quad 2\gamma_{r\varphi}=\frac{1}{r\sin\theta}\frac{\partial u_r}{\partial\varphi}+\frac{\partial u_\varphi}{\partial r}-\frac{u_\varphi}{r}\\
&2\gamma_{\theta\varphi}=\frac{1}{r}\frac{\partial u_\varphi}{\partial\theta}-\frac{u_\varphi}{r}\cot\theta+\frac{1}{r\sin\theta}\frac{\partial u_\theta}{\partial\varphi}\\
&E_r=-\frac{\partial\phi}{\partial r};\quad E_\theta=-\frac{1}{r}\frac{\partial\phi}{\partial\theta};\quad E_\varphi=-\frac{1}{r\sin\theta}\frac{\partial\phi}{\partial\varphi}\\
&H_r=-\frac{\partial\psi}{\partial r};\quad H_\theta=-\frac{1}{r}\frac{\partial\psi}{\partial\theta};\quad H_\varphi=-\frac{1}{r\sin\theta}\frac{\partial\psi}{\partial\varphi}
\end{aligned}
\tag{2}
$$

where u_i $(i=r, \theta, \varphi)$ are components of elastic displacement, ϕ and ψ are electric and magnetic potentials.

Under static deformation and in the absence of external forces, the equations of equilibrium are written in the following form:

$$
\begin{aligned}
&\frac{\partial\sigma_{rr}}{\partial r}+\frac{1}{r}\frac{\partial\sigma_{r\theta}}{\partial\theta}+\frac{1}{r\sin\theta}\frac{\partial\sigma_{r\varphi}}{\partial\varphi}+\frac{1}{r}(2\sigma_{rr}-\sigma_{\theta\theta}-\sigma_{\varphi\varphi}+\sigma_{r\theta}\cot\theta)=0\\
&\frac{\partial\sigma_{r\theta}}{\partial r}+\frac{1}{r}\frac{\partial\sigma_{\theta\theta}}{\partial\theta}+\frac{1}{r\sin\theta}\frac{\partial\sigma_{\theta\varphi}}{\partial\varphi}+\frac{1}{r}[(\sigma_{\theta\theta}-\sigma_{\varphi\varphi})\cot\theta+3\sigma_{r\theta}]=0\\
&\frac{\partial\sigma_{r\varphi}}{\partial r}+\frac{1}{r}\frac{\partial\sigma_{\theta\varphi}}{\partial\theta}+\frac{1}{r\sin\theta}\frac{\partial\sigma_{\varphi\varphi}}{\partial\varphi}+\frac{1}{r}(3\sigma_{r\varphi}+2\sigma_{\theta\varphi}\cot\theta)=0
\end{aligned}
\tag{3}
$$

Similarly, the static Maxwell equations of the electric and magnetic fields without electric and magnetic sources are given as

$$
\begin{aligned}
&\frac{\partial D_r}{\partial r}+\frac{1}{r}\frac{\partial D_\theta}{\partial\theta}+\frac{1}{r\sin\theta}\frac{\partial D_\varphi}{\partial\varphi}+\frac{1}{r}(2D_r+D_\theta\cot\theta)=0\\
&\frac{\partial B_r}{\partial r}+\frac{1}{r}\frac{\partial B_\theta}{\partial\theta}+\frac{1}{r\sin\theta}\frac{\partial B_\varphi}{\partial\varphi}+\frac{1}{r}(2B_r+B_\theta\cot\theta)=0
\end{aligned}
\tag{4}
$$

3. Spherical system of vector functions

To solve the problem described in Section 2, we introduce the following spherical system of vector functions (Ulitko, 1979):

$$
\begin{aligned}
&\boldsymbol{L}(\theta,\varphi;n,m)=\boldsymbol{e}_rS(\theta,\varphi;n,m)\\
&\boldsymbol{M}(\theta,\varphi;n,m)=r\nabla S=\left(\boldsymbol{e}_\theta\partial_\theta+\boldsymbol{e}_\varphi\frac{\partial_\varphi}{\sin\theta}\right)S(\theta,\varphi;n,m)\\
&\boldsymbol{N}(\theta,\varphi;n,m)=r\nabla\times(\boldsymbol{e}_rS)=(\boldsymbol{e}_\theta\frac{\partial_\varphi}{\sin\theta}-\boldsymbol{e}_\varphi\partial_\theta)S(\theta,\varphi;n,m)
\end{aligned}
\tag{5}
$$

where $\boldsymbol{e}_r$, $\boldsymbol{e}_\theta$, and $\boldsymbol{e}_\varphi$ are the unit vectors, respectively, along r-, θ- and φ-directions, and S is a scalar function defined by

$$
\begin{aligned}
S(\theta,\varphi;n,m)&=\sqrt{\frac{(2n+1)(n-m)!}{4\pi(n+m)!}}P_n^m(\cos\theta)e^{im\varphi},\\
&|m|\leqslant n \text{ and } n=0,1,2,\ldots
\end{aligned}
\tag{6}
$$

with P_n^m being the associated Legendre function (Abramovitz and Stegun, 1972). It is noted that the scalar function S satisfies the following Helmholtz equation

$$
\frac{1}{\sin\theta}\frac{\partial}{\partial\theta}\left(\sin\theta\frac{\partial S}{\partial\theta}\right)+\frac{1}{\sin^2\theta}\frac{\partial^2S}{\partial\varphi^2}+\lambda^2S=0 \tag{7a}
$$

or

$$
\frac{\partial S^2}{\partial\theta^2}+\cot\theta\frac{\partial S}{\partial\theta}+\frac{1}{\sin^2\theta}\frac{\partial^2S}{\partial\varphi^2}+\lambda^2S=0 \tag{7b}
$$

where $\lambda^2=n(n+1)$.

The following identity for any $f(\theta,\varphi)$ is also very useful when deriving our solutions

$$\frac{\partial}{\partial\theta}\left(\frac{1}{\sin\theta}\frac{\partial f}{\partial\varphi}\right)+\frac{\cot\theta}{\sin\theta}\frac{\partial f}{\partial\varphi}-\frac{1}{\sin\theta}\frac{\partial^2 f}{\partial\theta\partial\varphi}=0 \tag{8}$$

It is easy to show that the spherical system of vector functions (5) is complete and orthogonal in the following sense.

$$\begin{aligned}&\int_0^{2\pi}d\varphi\int_0^{\pi}\boldsymbol{L}(\theta,\varphi;n,m)\cdot\bar{\boldsymbol{L}}(\theta,\varphi;n',m')\sin\theta d\theta=\delta_{nn'}\delta_{mm'}\\&\int_0^{2\pi}d\varphi\int_0^{\pi}\boldsymbol{M}(\theta,\varphi;n,m)\cdot\bar{\boldsymbol{M}}(\theta,\varphi;n',m')\sin\theta d\theta=\lambda^2\delta_{nn'}\delta_{mm'}\\&\int_0^{2\pi}d\varphi\int_0^{\pi}\boldsymbol{N}(\theta,\varphi;n,m)\cdot\bar{\boldsymbol{N}}(\theta,\varphi;n',m')\sin\theta d\theta=\lambda^2\delta_{nn'}\delta_{mm'}\end{aligned} \tag{9}$$

where δ_{ij} are the components of the Kronecker delta and an overbar indicates complex conjugate.

4. Solutions in terms of spherical system of vector functions

4.1. Expansions of physical quantities in each spherical layer

Owing to the orthogonal properties (9), we can expand any vector, such as the elastic displacement $\boldsymbol{u}$, electric potential ϕ and magnetic potential ψ, as

$$\begin{aligned}&\boldsymbol{u}(r,\theta,\varphi)=\sum_{n=0}^{\infty}\sum_{m=-n}^{n}[U_L(r)\boldsymbol{L}(\theta,\varphi)+U_M(r)\boldsymbol{M}(\theta,\varphi)+U_N(r)\boldsymbol{N}(\theta,\varphi)]\\&=\sum_{n=0}^{\infty}\sum_{m=-n}^{n}\left[\boldsymbol{e}_\theta\left\{U_M(r)\partial_\theta+U_N(r)\frac{\partial_\varphi}{\sin\theta}\right\}+\boldsymbol{e}_\varphi\left\{U_M(r)\frac{\partial_\varphi}{\sin\theta}-U_N(r)\partial_\theta\right\}+\boldsymbol{e}_r U_L(r)\right]S(\theta,\varphi)\\&\phi(r,\theta,\varphi)=\sum_{n=0}^{\infty}\sum_{m=-n}^{n}\Phi(r)S(\theta,\varphi)\\&\psi(r,\theta,\varphi)=\sum_{n=0}^{\infty}\sum_{m=-n}^{n}\Psi(r)S(\theta,\varphi).\end{aligned} \tag{10}$$

For easy presentation, the scalar function $S(\theta, \varphi; n, m)$ is written as $S(\theta, \varphi)$ or S later on. For the same reason, the dependence of the expansion coefficients U_L, U_M, U_N, Φ and Ψ on (n,m) is also omitted.

Similarly, the traction vector $\boldsymbol{t}$, the electric displacement vector $\boldsymbol{D}$ and magnetic induction vector $\boldsymbol{B}$ can be expressed as

$$\begin{aligned}&\boldsymbol{t}(r,\theta,\varphi)\equiv\sigma_{rr}\boldsymbol{e}_r+\sigma_{r\theta}\boldsymbol{e}_\theta+\sigma_{r\varphi}\boldsymbol{e}_\varphi\\&\quad=\sum_{n=0}^{\infty}\sum_{m=-n}^{n}\left[\boldsymbol{e}_r T_L S+\boldsymbol{e}_\theta\left(T_M\frac{\partial S}{\partial\theta}+\frac{T_N}{\sin\theta}\frac{\partial S}{\partial\varphi}\right)+\boldsymbol{e}_\varphi\left(\frac{T_M}{\sin\theta}\frac{\partial S}{\partial\varphi}-T_N\frac{\partial S}{\partial\theta}\right)\right]\\&\boldsymbol{D}(r,\theta,\varphi)=\sum_{n=0}^{\infty}\sum_{m=-n}^{n}\left[\boldsymbol{e}_r D_L S+\boldsymbol{e}_\theta\left(D_M\frac{\partial S}{\partial\theta}+\frac{D_N}{\sin\theta}\frac{\partial S}{\partial\varphi}\right)+\boldsymbol{e}_\varphi\left(\frac{D_M}{\sin\theta}\frac{\partial S}{\partial\varphi}-D_N\frac{\partial S}{\partial\theta}\right)\right]\\&\boldsymbol{B}(r,\theta,\varphi)=\sum_{n=0}^{\infty}\sum_{m=-n}^{n}\left[\boldsymbol{e}_r B_L S+\boldsymbol{e}_\theta\left(B_M\frac{\partial S}{\partial\theta}+\frac{B_N}{\sin\theta}\frac{\partial S}{\partial\varphi}\right)+\boldsymbol{e}_\varphi\left(\frac{B_M}{\sin\theta}\frac{\partial S}{\partial\varphi}-B_N\frac{\partial S}{\partial\theta}\right)\right]\end{aligned} \tag{11}$$

Also in terms of the spherical system of vector functions, the strains, the electric and magnetic fields can be expressed by the coefficients of the elastic displacements and the electric and magnetic potentials

$$\gamma_{rr}=U_L'S;\quad \gamma_{\theta\theta}=\frac{U_L}{r}S+\frac{1}{r}\left(U_M\frac{\partial^2 S}{\partial\theta^2}+U_N\frac{\partial}{\partial\theta}\left[\frac{\partial S}{\sin\theta\partial\varphi}\right]\right) \tag{12a}$$

$$\gamma_{\varphi\varphi}=\frac{U_L}{r}S+\frac{1}{r\sin\theta}\left(\frac{U_M}{\sin\theta}\frac{\partial^2 S}{\partial\varphi^2}-U_N\frac{\partial S^2}{\partial\theta\partial\varphi}\right)+\frac{\cot\theta}{r}\left(U_M\frac{\partial S}{\partial\theta}+\frac{U_N}{\sin\theta}\frac{\partial S}{\partial\varphi}\right) \tag{12b}$$

$$2\gamma_{r\theta}=\frac{U_L}{r}\frac{\partial S}{\partial\theta}+\left(U_M'\frac{\partial S}{\partial\theta}+\frac{U_N'}{\sin\theta}\frac{\partial S}{\partial\varphi}\right)-\left(U_M\frac{1}{r}\frac{\partial S}{\partial\theta}+\frac{U_N}{r\sin\theta}\frac{\partial S}{\partial\varphi}\right) \tag{12c}$$

$$2\gamma_{r\varphi}=\frac{1}{r\sin\theta}U_L\frac{\partial S}{\partial\varphi}+\left(\frac{U_M'}{\sin\theta}\frac{\partial S}{\partial\varphi}-U_N'\frac{\partial S}{\partial\theta}\right)-\left(\frac{U_M}{r\sin\theta}\frac{\partial S}{\partial\varphi}-U_N\frac{1}{r}\frac{\partial S}{\partial\theta}\right) \tag{12d}$$

$$2\gamma_{\theta\varphi}=\frac{1}{r}\left(U_M\frac{\partial}{\partial\theta}\left[\frac{1}{\sin\theta}\frac{\partial S}{\partial\varphi}\right]-U_N\frac{\partial^2 S}{\partial\theta^2}\right)-\frac{\cot\theta}{r}\left(\frac{U_M}{\sin\theta}\frac{\partial S}{\partial\varphi}-U_N\frac{\partial S}{\partial\theta}\right)+\frac{1}{r\sin\theta}\left(U_M\frac{\partial^2 S}{\partial\theta\partial\varphi}+\frac{U_N}{\sin\theta}\frac{\partial^2 S}{\partial\varphi^2}\right) \tag{12e}$$

$$E_r=-\Phi' S;\quad E_\theta=-\frac{\Phi}{r}\frac{\partial S}{\partial\theta};\quad E_\varphi=-\frac{\Phi}{r\sin\theta}\frac{\partial S}{\partial\varphi} \tag{12f}$$

$$H_r=-\Psi' S;\quad H_\theta=-\frac{\Psi}{r}\frac{\partial S}{\partial\theta};\quad H_\varphi=-\frac{\Psi}{r\sin\theta}\frac{\partial S}{\partial\varphi} \tag{12g}$$

in which the superscript prime "′" indicates the derivative with respect to the radial coordinate r.

Substituting Eqs. (11) and (12) into Eq. (1) and comparing the coefficients on both sides of the resulting equations, we find

$$\begin{aligned}T_L&=2c_{13}\frac{U_L}{r}-\lambda^2 c_{13}\frac{U_M}{r}+c_{33}U_L'+e_{33}\Phi'+q_{33}\Psi'\\T_M&=c_{44}\left(\frac{U_L}{r}+U_M'-\frac{U_M}{r}\right)+e_{15}\frac{\Phi}{r}+q_{15}\frac{\Psi}{r}\\T_N&=c_{44}\left(U_N'-\frac{U_N}{r}\right)\\D_L&=2e_{31}\frac{U_L}{r}-\lambda^2 e_{31}\frac{U_M}{r}+e_{33}U_L'-\varepsilon_{33}\Phi'-\alpha_{33}\Psi'\\B_L&=2q_{31}\frac{U_L}{r}-\lambda^2 q_{31}\frac{U_M}{r}+q_{33}U_L'-\alpha_{33}\Phi'-\mu_{33}\Psi'\end{aligned} \tag{13}$$

Furthermore, making use of Eqs. (1)–(4) and (11), we obtain

$$\begin{aligned}&T_L'-\lambda^2\frac{T_M}{r}+\frac{2T_L}{r}-\frac{1}{r}(2c_{13}U_L'-2e_{31}\Phi'-2q_{31}\Psi')-\frac{2U_L}{r^2}C+\frac{1}{r^2}C\lambda^2U_M=0\\&T_M'+\frac{3}{r}T_M+\frac{1}{r}(c_{13}U_L'+e_{31}\Phi'+q_{31}\Psi')+\frac{1}{r^2}CU_L+\frac{U_M}{r^2}\{2c_{66}(1-\lambda^2)-\lambda^2c_{12}\}=0\\&T_N'+\frac{3}{r}T_N+\frac{1}{r^2}U_Nc_{66}(2-\lambda^2)=0\\&D_L'-\lambda^2\frac{e_{15}}{r}\left(\frac{1}{r}U_L+U_M'-\frac{U_M}{r}-\frac{\varepsilon_{11}}{e_{15}}\frac{1}{r}\Phi-\frac{\alpha_{11}}{e_{15}}\frac{1}{r}\Psi\right)+\frac{2}{r}D_L=0\\&B_L'-\lambda^2\frac{q_{15}}{r}\left(\frac{1}{r}U_L+U_M'-\frac{U_M}{r}-\frac{\alpha_{11}}{q_{15}}\frac{1}{r}\Phi-\frac{\mu_{11}}{q_{15}}\frac{1}{r}\Psi\right)+\frac{2}{r}B_L=0\end{aligned} \tag{14}$$

where $C=c_{11}+c_{12}$.

It is obvious from Eqs. (13) and (14) that T_N and U_N are uncoupled form other variables and that they are purely elastic, meaning that they are independent of the electric and magnetic fields. We call this the N-type problem, which is also associated with the torsional deformation only. The N-type problem satisfies the following set of first-order differential equations

$$\begin{bmatrix}U_N'\\T_N'\end{bmatrix}=\begin{bmatrix}1/r & 1/c_{44}\\-\frac{c_{66}}{r^2}(2-\lambda^2) & -3/r\end{bmatrix}\begin{bmatrix}U_N\\T_N\end{bmatrix} \tag{15}$$

The remaining part is called LM-type problem, which couples the elastic, electric and magnetic fields together. The deformation in this case is associated with the spheroidal deformation. It is governed by the following set of first-order differential equations

$$\begin{bmatrix}\boldsymbol{R}_{11} & \boldsymbol{0}\\\boldsymbol{R}_{21} & r\boldsymbol{I}\end{bmatrix}\begin{bmatrix}\boldsymbol{U}'\\\boldsymbol{T}'\end{bmatrix}=\begin{bmatrix}\boldsymbol{H}_{11}/r & \boldsymbol{I}\\\boldsymbol{H}_{21}/r & \boldsymbol{H}_{22}\end{bmatrix}\begin{bmatrix}\boldsymbol{U}\\\boldsymbol{T}\end{bmatrix} \tag{16}$$

in which each sub-matrix is given by

$$\boldsymbol{U}=[U_L\quad U_M\quad\Phi\quad\Psi]^t;\quad \boldsymbol{T}=[T_L\quad T_M\quad D_L\quad B_L]^t \tag{17a}$$

$$\boldsymbol{R}_{11}=\begin{bmatrix}c_{33}&0&e_{33}&q_{33}\\0&c_{44}&0&0\\e_{33}&0&-\varepsilon_{33}&-\alpha_{33}\\q_{33}&0&-\alpha_{33}&-\mu_{33}\end{bmatrix};\quad \boldsymbol{R}_{21}=\begin{bmatrix}-2c_{13}&0&2e_{31}&2q_{31}\\c_{13}&0&e_{31}&q_{31}\\0&-\lambda^2e_{15}&0&0\\0&-\lambda^2q_{15}&0&0\end{bmatrix} \tag{17b}$$

$$\boldsymbol{H}_{11}=\begin{bmatrix}-2c_{13} & \lambda^2 c_{13} & 0 & 0\\ -c_{44} & c_{44} & -e_{15} & -q_{15}\\ -2e_{31} & \lambda^2 e_{31} & 0 & 0\\ -2q_{31} & \lambda^2 q_{31} & 0 & 0\end{bmatrix} \tag{17c}$$

$$\boldsymbol{H}_{21}=\begin{bmatrix}2C & -\lambda^2 C & 0 & 0\\ -C & -2c_{66}[1-\lambda^2]+\lambda^2 c_{12} & 0 & 0\\ \lambda^2 e_{15} & -\lambda^2 e_{15} & -\lambda^2\varepsilon_{11} & -\lambda^2\alpha_{11}\\ \lambda^2 q_{15} & -\lambda^2 q_{15} & -\lambda^2\alpha_{11} & -\lambda^2\mu_{11}\end{bmatrix};$$

$$\boldsymbol{H}_{22}=\begin{bmatrix}-2 & \lambda^2 & 0 & 0\\ 0 & -3 & 0 & 0\\ 0 & 0 & -2 & 0\\ 0 & 0 & 0 & -2\end{bmatrix} \tag{17d}$$

Both Eq. (15) for the N-type and (16) for the LM-type are first-order differential equations with variable coefficients. In other words, their coefficients are functions of the variable r. To find the general solutions to these equations, we first recast Eqs. (15) and (16) into

$$\begin{bmatrix}rU_N'\\ r^2T_N'\end{bmatrix}=\begin{bmatrix}1 & 1/c_{44}\\ -c_{66}(2-\lambda^2) & -3\end{bmatrix}\begin{bmatrix}U_N\\ rT_N\end{bmatrix}$$
$$\begin{bmatrix}\boldsymbol{R}_{11} & \boldsymbol{0}\\ \boldsymbol{R}_{21} & I\end{bmatrix}\begin{bmatrix}r\boldsymbol{U}'\\ r^2\boldsymbol{T}'\end{bmatrix}=\begin{bmatrix}\boldsymbol{H}_{11} & I\\ \boldsymbol{H}_{21} & \boldsymbol{H}_{22}\end{bmatrix}\begin{bmatrix}\boldsymbol{U}\\ r\boldsymbol{T}\end{bmatrix} \tag{18}$$

To solve Eq. (18), we let $r=r_i e^{\xi}$, with $0\leqslant\xi\leqslant\xi_i$ and $\xi_i=\ln(r_{i+1}/r_i)$ to change Eq. (18) to (derivative is now with respect to ξ)

$$\begin{bmatrix}U_N'\\ rT_N'\end{bmatrix}=\begin{bmatrix}1 & 1/c_{44}\\ -c_{66}(2-\lambda^2) & -3\end{bmatrix}\begin{bmatrix}U_N\\ rT_N\end{bmatrix}$$
$$\begin{bmatrix}\boldsymbol{R}_{11} & \boldsymbol{0}\\ \boldsymbol{R}_{21} & I\end{bmatrix}\begin{bmatrix}\boldsymbol{U}'\\ r\boldsymbol{T}'\end{bmatrix}=\begin{bmatrix}\boldsymbol{H}_{11} & I\\ \boldsymbol{H}_{21} & \boldsymbol{H}_{22}\end{bmatrix}\begin{bmatrix}\boldsymbol{U}\\ r\boldsymbol{T}\end{bmatrix} \tag{19}$$

Introducing

$$\bar{T}_N=rT_N;\quad \bar{\boldsymbol{T}}=r\boldsymbol{T} \tag{20}$$

we obtain the following first-order differential equations with constant coefficients

$$\begin{bmatrix}U_N'\\ \bar{T}_N'\end{bmatrix}=\boldsymbol{B}^N\begin{bmatrix}U_N\\ \bar{T}_N\end{bmatrix}$$
$$\begin{bmatrix}\boldsymbol{U}'\\ \bar{\boldsymbol{T}}'\end{bmatrix}=\boldsymbol{B}\begin{bmatrix}\boldsymbol{U}\\ \bar{\boldsymbol{T}}\end{bmatrix} \tag{21}$$

In Eq. (21),

$$\boldsymbol{B}^N=\begin{bmatrix}1 & 1/c_{44}\\ -c_{66}(2-\lambda^2) & -2\end{bmatrix}$$
$$\boldsymbol{B}=\begin{bmatrix}\boldsymbol{R}_{11}^{-1} & \boldsymbol{0}\\ -\boldsymbol{R}_{21}\boldsymbol{R}_{11}^{-1} & \boldsymbol{I}\end{bmatrix}\begin{bmatrix}\boldsymbol{H}_{11} & \boldsymbol{I}\\ \boldsymbol{H}_{21} & \boldsymbol{H}_{22}+\boldsymbol{I}\end{bmatrix} \tag{22}$$

4.2. Solution and propagation matrices of N- and LM-type deformations

4.2.1. Spherically symmetric deformation

Before we present the solutions to Eq. (21) and the corresponding propagation matrices, we first discuss the special and simple deformation corresponding to $n=0$ and $m=0$ in our spherical system of vector functions. It is obvious that for this case we do not have the N-type solution, and that the LM-type solution is reduced to the solution associated with L component only. More specifically, when $n=0$, we find that Eq. (16) needs to be reorganized by introducing the extended displacements and tractions as

$$\boldsymbol{U}=[U_L,\Phi,\Psi]^t;\quad \boldsymbol{T}=[T_L,D_L,B_L]^t \tag{23}$$

This is equivalent to removing the second row and second column in the involved matrices while also letting $n=0$ in other elements. Thus, the size of the matrices defined in Eq. (17) will all be reduced to 3×3, with the following new elements

$$\boldsymbol{R}_{11}=\begin{bmatrix}c_{33} & e_{33} & q_{33}\\ e_{33} & -\varepsilon_{33} & -\alpha_{33}\\ q_{33} & -\alpha_{33} & -\mu_{33}\end{bmatrix};\quad \boldsymbol{R}_{21}=\begin{bmatrix}-2c_{13} & 2e_{31} & 2q_{31}\\ 0 & 0 & 0\\ 0 & 0 & 0\end{bmatrix} \tag{24a}$$

$$\boldsymbol{H}_{11}=\begin{bmatrix}-2c_{13} & 0 & 0\\ -2e_{31} & 0 & 0\\ -2q_{31} & 0 & 0\end{bmatrix};\quad \boldsymbol{H}_{21}=\begin{bmatrix}2C & 0 & 0\\ 0 & 0 & 0\\ 0 & 0 & 0\end{bmatrix};$$
$$\boldsymbol{H}_{22}=\begin{bmatrix}-2 & 0 & 0\\ 0 & -2 & 0\\ 0 & 0 & -2\end{bmatrix} \tag{24b}$$

Therefore, instead of a 4×4 system, for the special case of $n=0$, all the involved intermediate matrices are 3×3. We also point out that since $n=1$ involves rigid-body motion (Watson and Singh, 1972), its solution will not be discussed in this paper.

4.2.2. Solution matrices and propagation matrices

We present the solutions and propagation matrices for both the N-type and LM-type. For the LM-type the solution corresponding to $n=0$ will be formally the same as for the case of $n\geqslant2$, but with the involved vector and matrix sizes being reduced, and with the intermediate matrices for $n=0$ being those given by Eq. (24).

For each given layer with constant material properties, the solutions of Eq. (21) can be assumed as

$$\begin{bmatrix}U_N(\xi)\\ \bar{T}_N(\xi)\end{bmatrix}=\exp(\boldsymbol{B}^N\xi)\begin{bmatrix}U_N(0)\\ \bar{T}_N(0)\end{bmatrix}$$
$$\begin{bmatrix}\boldsymbol{U}(\xi)\\ \bar{\boldsymbol{T}}(\xi)\end{bmatrix}=\exp(\boldsymbol{B}\xi)\begin{bmatrix}\boldsymbol{U}(0)\\ \bar{\boldsymbol{T}}(0)\end{bmatrix} \tag{25}$$

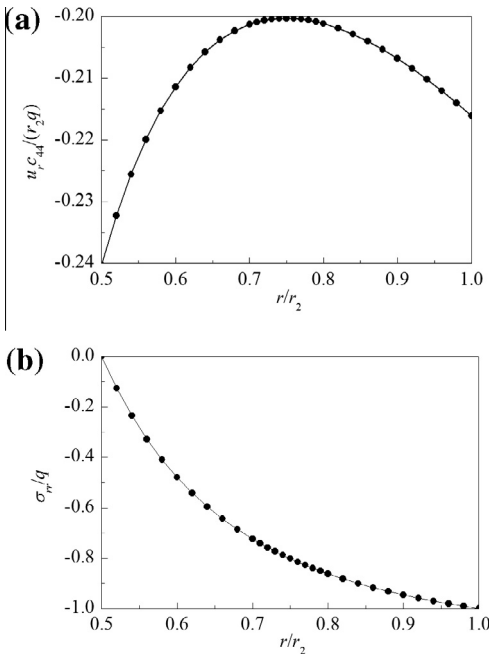

Fig. 2. Variation of the dimensionless elastic displacement component $u_r c_{44}/(qr_2)$ in (a) and the dimensionless stress component $\sigma_{rr}/(qc_{44})$ in (b) along the radial direction (r/r_2) in a spherically anisotropic piezoelectric hollow sphere made of $BaTiO_3$ under a uniform external pressure q on its outer surface r_2. The electric shorted circuit is applied on both the inner $(r=r_1)$ and outer $(r=r_2)$ surfaces.

Table 1
Material properties of piezoelectric $BaTiO_3$, magnetic $CoFe_2O_4$, and MEE materials MEE which is made of 50% $BaTiO_3$ and 50% $CoFe_2O_4$ (c_{ij} in 10^9 N/m^2, e_{ij} in C/m^2, q_{ij} in N/Am, ε_{ij} in 10^{-9} C^2/(Nm^2), μ_{ij} in 10^{-6} Ns^2/C^2, α_{ij} in 10^{-12} Ns/VC).

Properties	$BaTiO_3$	$CoFe_2O_4$	MEE	Properties	$BaTiO_3$	$CoFe_2O_4$	MEE
c_{11}	166	286	213	$e_{31}=e_{32}$	−4.4	0	−2.71
c_{22}	166	286	213	e_{33}	18.6	0	8.86
c_{12}	77	173	113	$e_{24}=e_{15}$	11.6	0	0.15
c_{13}	78	170.5	113	$q_{31}=q_{32}$	0	580.3	222
c_{23}	78	170.5	113	q_{33}	0	699.7	292
c_{33}	162	269.5	207	$q_{24}=q_{15}$	0	550	185
c_{44}	43	45.3	49.9	$\varepsilon_{11}=\varepsilon_{22}$	11.2	0.08	0.24
c_{55}	43	45.3	49.9	ε_{33}	12.6	0.093	6.37
c_{66}	44.5	56.5	50	$\mu_{11}=\mu_{22}$	5	590	201
α_{11}	0	0	−5.23	μ_{33}	10	157	83.9
α_{33}	0	0	2750	–	–	–	–

For ith layer, with its inner and outer interfaces at $r=r_i$ and r_{i+1}, which corresponds 0 and ξ_i, the extended displacement and traction components at its interfaces are connected by

$$\begin{bmatrix} U_N(\xi_i) \\ \bar{T}_N(\xi_i) \end{bmatrix} = \exp(\boldsymbol{B}_i^N \xi_i) \begin{bmatrix} U_N(0) \\ \bar{T}_N(0) \end{bmatrix} = \exp(\boldsymbol{B}_i^N \xi_i) \begin{bmatrix} U_N(\xi_{i-1}) \\ \bar{T}_N(\xi_{i-1}) \end{bmatrix}$$
$$\begin{bmatrix} \boldsymbol{U}(\xi_i) \\ \bar{\boldsymbol{T}}(\xi_i) \end{bmatrix} = \exp(\boldsymbol{B}_i \xi_i) \begin{bmatrix} \boldsymbol{U}(0) \\ \bar{\boldsymbol{T}}(0) \end{bmatrix} = \exp(\boldsymbol{B}_i \xi_i) \begin{bmatrix} \boldsymbol{U}(\xi_{i-1}) \\ \bar{\boldsymbol{T}}(\xi_{i-1}) \end{bmatrix} \tag{26}$$

We point out that there is no summation over the repeated index i on the right-hand side of Eq. (26). With the relation (26), we can propagate the solution from the inner surface (r_1, $\xi=0$) to the outer surface (r_{p+1}, $\xi_p=\ln(r_{p+1}/r_p)$) of the layered MEE hollow sphere to arrive at

$$\begin{bmatrix} U_N(\xi_p) \\ \bar{T}_N(\xi_p) \end{bmatrix} = \boldsymbol{p}^N \begin{bmatrix} U_N(0) \\ \bar{T}_N(0) \end{bmatrix}$$
$$\begin{bmatrix} \boldsymbol{U}(\xi_p) \\ \bar{\boldsymbol{T}}(\xi_p) \end{bmatrix} = \boldsymbol{p} \begin{bmatrix} \boldsymbol{U}(0) \\ \bar{\boldsymbol{T}}(0) \end{bmatrix} \tag{27}$$

where

$$\boldsymbol{p}^N = \exp(\boldsymbol{B}_p^N \xi_p) \exp(\boldsymbol{B}_{p-1}^N \xi_{p-1}) \dots \exp(\boldsymbol{B}_1^N \xi_1)$$
$$\boldsymbol{p} = \exp(\boldsymbol{B}_p \xi_p) \exp(\boldsymbol{B}_{p-1} \xi_{p-1}) \dots \exp(\boldsymbol{B}_1 \xi_1) \tag{28}$$

Eq. (27) is a simple relation and, for given boundary conditions on both the inner and outer surfaces, can be solved for the involved unknowns. We present the following example for the LM-type to illustrate.

We assume that, at the outer surface $r=r_{p+1}$, the radial traction in its dimensionless form is applied, as

$$\sigma_{rr} = \sigma_0 P_n(\cos\theta)/c_{\max} \tag{29}$$

where $c_{\max}$ is the maximum value of all elastic coefficients among all layers and P_n represents the n-order Legendre function. In addition, we assume that all other elastic traction components on both the inner and outer surfaces are zero and the electric and magnetic fields are short circuited at those locations (i.e., $\Phi(r_1)=\Phi(r_{p+1})=\Psi(r_1)=\Psi(r_{p+1})=0$).

Then, Eq. (27) for the LM-type can be written as

$$\begin{bmatrix} \boldsymbol{U}_1(\xi_p) \\ \boldsymbol{0} \\ r_{p+1}\bar{\sigma}_{rr} \\ \bar{\boldsymbol{T}}_2(\xi_p) \end{bmatrix} = \begin{bmatrix} \boldsymbol{p}_{11} & \boldsymbol{p}_{12} & \boldsymbol{p}_{13} & \boldsymbol{p}_{14} \\ \boldsymbol{p}_{21} & \boldsymbol{p}_{22} & \boldsymbol{p}_{23} & \boldsymbol{p}_{24} \\ \boldsymbol{p}_{31} & \boldsymbol{p}_{32} & \boldsymbol{p}_{33} & \boldsymbol{p}_{34} \\ \boldsymbol{p}_{41} & \boldsymbol{p}_{42} & \boldsymbol{p}_{43} & \boldsymbol{p}_{44} \end{bmatrix} \begin{bmatrix} \boldsymbol{U}_1(0) \\ \boldsymbol{0} \\ \boldsymbol{0} \\ \bar{\boldsymbol{T}}_2(0) \end{bmatrix} \tag{30}$$

in which $\bar{\sigma}_{rr}=\sigma_0/c_{\max}$, $\boldsymbol{U}_1=[U_L \quad U_M]^t$, $\bar{\boldsymbol{T}}_2=[rD_L \quad rB_L]^t$. From Eq. (30), one can determine the unknowns at the inner surface $r=r_1$ as

$$\begin{bmatrix} \boldsymbol{U}_1(0) \\ \bar{\boldsymbol{T}}_2(0) \end{bmatrix} = \begin{bmatrix} \boldsymbol{p}_{21} & \boldsymbol{p}_{24} \\ \boldsymbol{p}_{31} & \boldsymbol{p}_{34} \end{bmatrix}^{-1} \begin{bmatrix} \boldsymbol{0} \\ r_{p+1}\bar{\sigma}_{rr} \end{bmatrix} \tag{31}$$

With the solved coefficients at the inner surface, a propagating relation similar to Eq. (26) can be applied to find the expansion coefficients at any r-level in any given layer. For instance, to obtain the coefficients of the extended displacement and traction vectors at r, with $r_{j-1}<r<r_j$ in layer j, we propagate the solution from the inner surface to find

$$\begin{bmatrix} \boldsymbol{U}(\xi) \\ \bar{\boldsymbol{T}}(\xi) \end{bmatrix} = \exp(\boldsymbol{B}_j \xi) \exp(\boldsymbol{B}_{j-1}\xi_{j-1}) \dots \exp(\boldsymbol{B}_1 \xi_1) \begin{bmatrix} \boldsymbol{U}(0) \\ \bar{\boldsymbol{T}}(0) \end{bmatrix} \tag{32}$$

Substituting the expansion coefficients from Eq. (32) into Eqs. (10) and (11), we can then obtain the extended displacements and tractions at any r-level in any layer as functions of spherical coordinates (r, θ, φ). Thus, the boundary value problem is finally solved.

5. Numerical examples

5.1. Verification of the analytical solution

Before presenting the numerical results, we have first compared our solution to existing solutions for the reduced cases. We apply our formulation to the reduced piezoelectric case where a piezoelectric hollow sphere is made of $BaTiO_3$ with its inner radius, r_1, being half of its outer radius r_2. It is assumed that the short-circuited electric boundary condition is applied to both the inner and outer surfaces and that a uniform external pressure q (i.e., $\sigma_{rr}=-q$) is applied on the outer surface of the sphere while other elastic traction components are zero on both the inner and outer surfaces. The material coefficients of the piezoelectric $BaTiO_3$ are the same as those in Chen and co-workers (2001). Fig. 2a and b show the distribution of the dimensionless stress $\sigma_{rr}/(qc_{44})$ and the dimensionless displacement $u_r c_{44}/(qr_2)$. These distributions are identical to those of Chen and co-workers (2001).

5.2. A hollow sandwich sphere under uniform external pressure

Having validated our solutions, we now apply them to a three-layered sandwich hollow sphere made of magneto-electro-elastic materials. We first consider the spherically symmetric deformation corresponding to $n=0$. The following three different stacking sequences are studied (from inner layer to the outer layer): (1) B/F/B, (2) F/B/F, (3) MEE/MEE/MEE (simply MEE), where "B" denotes BaTiO3, "F" denotes $CoFe_2O_4$, and "MEE" denotes the MEE material made of 50% BaTiO3 and 50% $CoFe_2O_4$. The third case actually corresponds to a homogeneous spherical shell made of the coupled MEE material. We denote the outer radius of the layered hollow sphere by $r_4=R$, and let the inner radius of the hollow sphere be located at $r_1=0.4R$ with each of the three layers having equal thickness of $0.2R$. The material constants are listed in Table.1 and are taken from Chen and co-workers (2007a,b) and Xue and Pan (2013) with the MEE material properties being predicted based

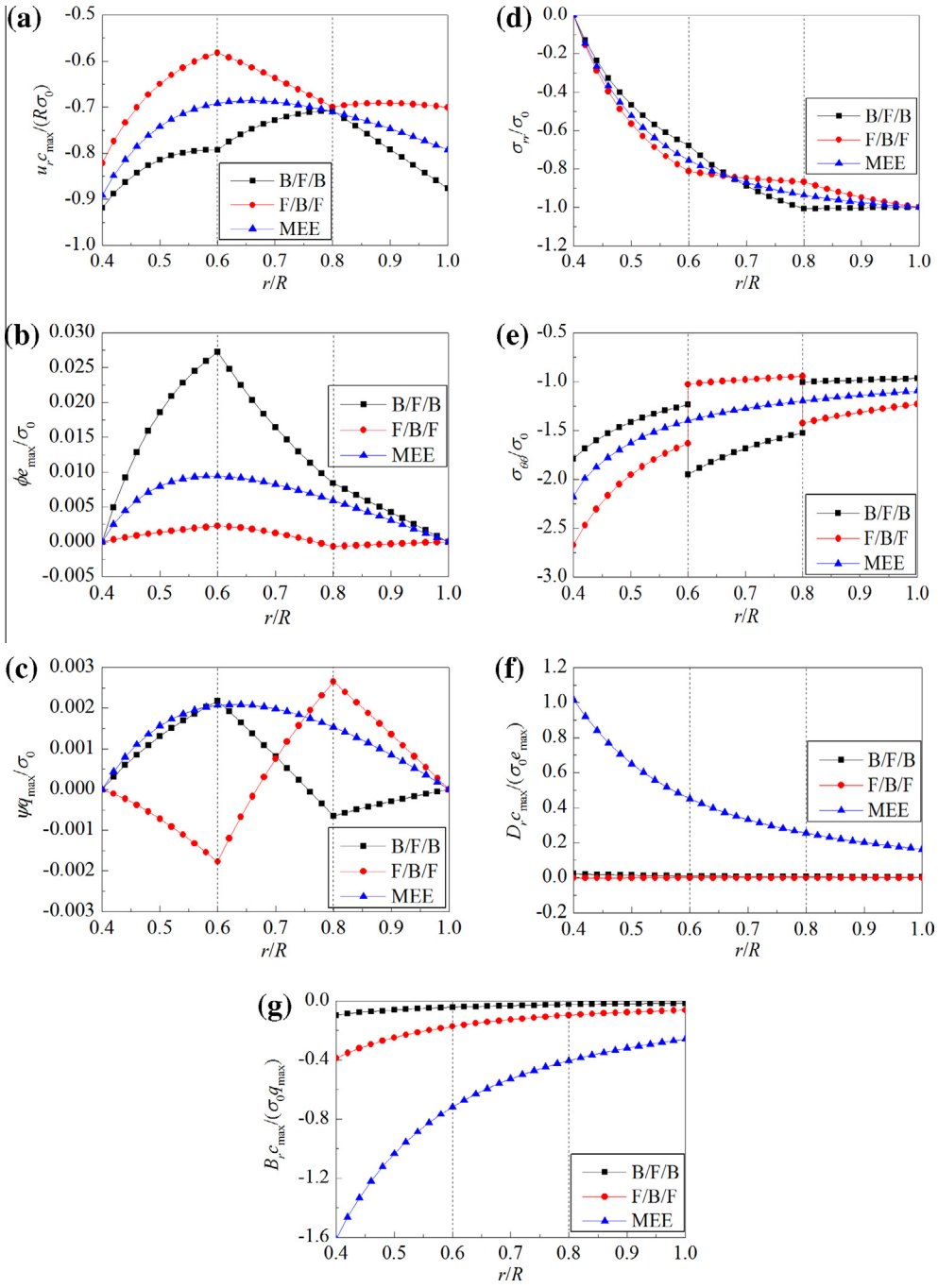

Fig. 3. Variation of the extended displacements and stresses along the radial direction of the hollow sandwich sphere made of magneto-electro-elastic materials with its outer surface being under uniform pressure $p = \sigma_0/c_{max}$. The dimensionless elastic displacement component $u_r c_{max}/(R\sigma_0)$ in (a), electric potential $\phi e_{max}/\sigma_0$ in (b), magnetic potential $\psi q_{max}/\sigma_0$ in (c), radial stress σ_{rr}/σ_0 in (d), circumferential stress $\sigma_{\theta\theta}/\sigma_0$ in (e), radial electric displacement $D_r c_{max}/(\sigma_0 e_{max})$ in (f), and radial magnetic induction $B_r c_{max}/(\sigma_0 q_{max})$ in (g). The dashed thin vertical lines denote the two interfaces in the sandwich sphere.

on the micromechanics of Kuo and Pan (2011). As for boundary conditions, we assume that the outer surface of the sphere is under a uniform external pressure, i.e., $\sigma_{rr} = -\sigma_0$ and that the other elastic traction components are zero on both the inner and outer surfaces of the layered sphere. Furthermore, electric and magnetic short-circuit is assumed on both the inner and outer surfaces. For easy presentation, all quantities are normalized by following the same approach used in Chen and co-workers (2007a,b).

Fig. 3 show the variation of the induced extended displacements and stresses in dimensionless form with respect to the normalized radius r/R. The elastic displacement component $u_r c_{max}/(R\sigma_0)$ is presented in Fig. 3a, the electric potential $\phi e_{max}/\sigma_0$ in Fig. 3b, the magnetic potential $\psi q_{max}/\sigma_0$ in Fig. 3c, the radial traction σ_{rr}/σ_0 in Fig. 3d, the circumferential traction $\sigma_{\theta\theta}/\sigma_0$ in Fig. 3e, the radial electric displacement $D_r c_{max}/(\sigma_0 e_{max})$ in Fig. 3f, and the radial magnetic induction $B_r c_{max}/(\sigma_0 q_{max})$ in Fig. 3g. While c_{max} is the maximum elastic coefficients among all materials, e_{max} and q_{max} are, respectively, the maximum absolute values of the piezoelectric and magnetostrictive coefficients of the given materials. From Fig. 3a–c, by comparing to the homogeneous MEE results,

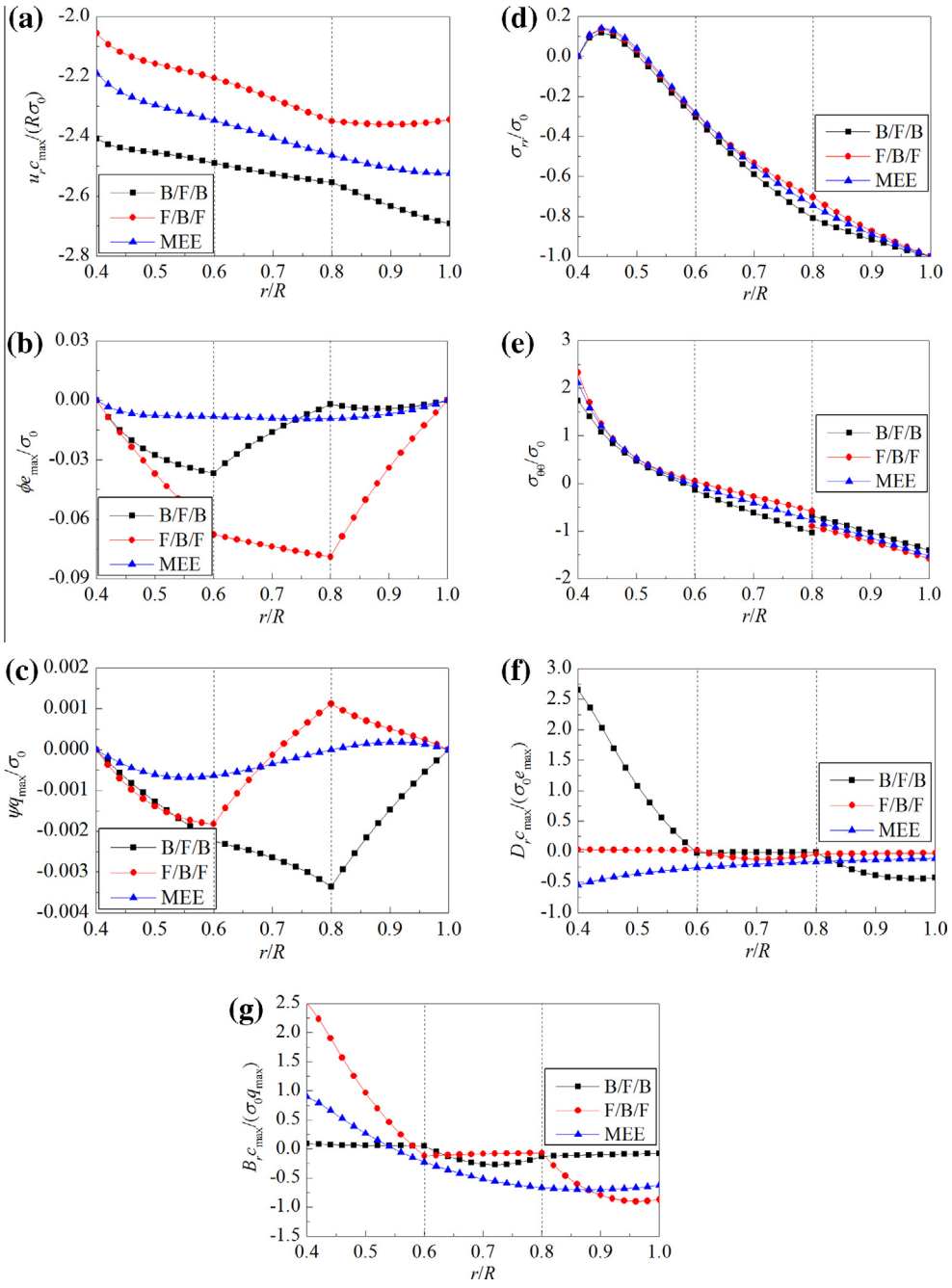

Fig. 4. Variation of the extended displacements and stresses along the radial direction at fixed $\theta = 0°$ of the hollow sandwich sphere made of magneto-electro-elastic materials with its outer surface being under an axisymmetric external pressure $\sigma_{rr} = \sigma_0 P_2(\cos\theta)/c_{max}$. The dimensionless elastic displacement component $u_r c_{max}/(R\sigma_0)$ in (a), electric potential $\phi e_{max}/\sigma_0$ in (b), magnetic potential $\psi q_{max}/\sigma_0$ in (c), radial stress σ_{rr}/σ_0 in (d), circumferential stress $\sigma_{\theta\theta}/\sigma_0$ in (e), radial electric displacement $D_r c_{max}/(\sigma_0 e_{max})$ in (f), and radial magnetic induction $B_r c_{max}/(\sigma_0 q_{max})$ in (g). The dashed thin vertical lines denote the two interfaces in the sandwich sphere.

the elastic displacement and electric and magnetic potentials are clearly affected by the layering. From Fig. 3d, we can observe that the radial stress is only slightly influenced by the layering and that the traction boundary condition is satisfied which verifies again our solution. The circumferential stress, however, shows obvious dependence on layering as can be observed from Fig. 3e, along with its expected jump across the interfaces. It is particularly interesting that, while the magnetostrictive layer F corresponds to a large increase in the stress magnitude in the middle layer of the sandwich B/F/B, the piezoelectric layer B helps to reduce it substantially in the middle layer of the sandwich F/B/F. From Fig. 3f and g, we observe that, compared to the semi-coupled B/F/B or F/B/F cases, the truly coupled MEE layer would induce much large magnitude of the electric displacement and magnetic induction, which is particular true in the inner layer.

5.3. A hollowed sandwich sphere under an axisymmetric external pressure

Here we assume the same sandwich structure as in Section 5.2, but under an axisymmetric external pressure $\sigma_{rr} = \sigma_0 P_2(\cos\theta)/c_{max}$ on its outer surface. The response of the layered sphere is plotted along the radial direction for fixed angle $\theta = 0°$. Fig. 4 shows that distribution of the extended displacements and stresses along

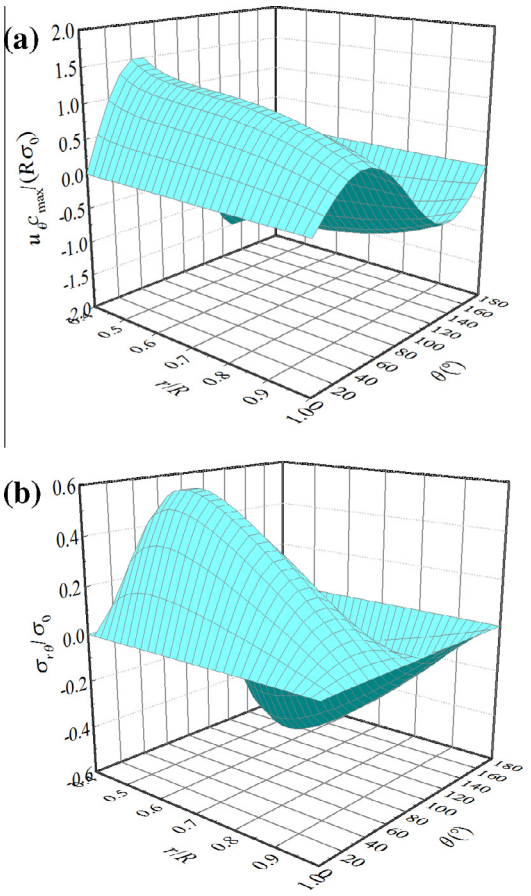

Fig. 5. Distribution of dimensionless displacement component $u_\theta c_{\max}/(R/\sigma_0)$ in (a) and stress component $\sigma_{r\theta}/\sigma_0$ in (b) as functions of (r,θ) in the homogeneous MEE hollow sphere under an axisymmetric external pressure $\sigma_{rr} = \sigma_0 P_2(\cos\theta)/c_{\max}$ applied on its outer surface $r = R$.

radial direction in the same sandwich hollow spheres as in Fig. 3 discussed in Section 5.2. Similar to Fig. 3, the extended displacements (i.e., radial elastic displacement in Fig. 4a, electric potential in Fig. 4b, and magnetic potential in Fig. 4c) depend significantly upon layering of the sphere, but the radial stress component is nearly independent of layering and MEE coupling. Furthermore, for the order 2 case, material layering has only slight effect on the circumferential stress, even though one can still observe its discontinuities across the interface of different layers (Fig. 4e). Comparing the electric displacement and magnetic induction for orders 0 and 2 (i.e., Figs. 3f and g vs. 4f and g), one can clearly notice the difference. While for the case of order 0, the largest magnitude of these electric and magnetic quantities is reached on the inner surface ($r/R = 0.4$) by the fully coupled homogeneous MEE hollow sphere (Fig. 3f and g), for the case of order 2, the B/F/B sandwich sphere has the largest magnitude of the electric displacement on the inner surface (Fig. 4f) and the F/B/F sandwich sphere has the largest magnitude of the magnetic induction on the inner surface (Fig. 4g).

Shown in Fig. 5a and b are the variations of the elastic displacement component u_θ and the stress component $\sigma_{r\theta}$ in both the radial and circumferential directions when the upper surface of the homogeneous hollow MEE sphere is under the same axisymmetric external pressure of order 2 as in Fig. 4. These two figures illustrate how the elastic displacement and stress vary as functions of (r, θ). While these 3D contour plots are smooth, there are minima and maxima within the (r, θ)-plane one may need to pay attention to, as can be clearly observed from Fig. 5b for the shear stress distribution.

6. Conclusions

In this paper, we have derived the analytical solutions for a layered hollow sphere made of spherically anisotropic magneto-electro-elastic materials. The spherical system of vector functions is introduced to express the solutions and variable transformation is carried out twice in order to reduce the system of differential equations to a standard one with constant coefficients. For the multilayered case, the propagator matrix method is employed with the propagating matrix in each layer being simply the exponential matrix. We further point out that under the spherical system of vector functions, the spheroidal and torsional deformations can be easily separated with the multiphase coupling being involved in the spheroidal deformation only. The special case of uniform deformation corresponding to order 0 is also discussed. As numerical examples, we have presented the results for both orders 0 and 2 for three layered hollow spheres made of piezoelectric $BaTiO_3$, magnetostrictive $CoFe_2O_4$, and the coupled MEE material under external pressures of orders 0 and 2. The stacking sequences studied are B/F/B, F/B/F, and the homogenous MEE spheres. The influence of layering, multiphase coupling, as well as different orders of loading, on the elastic, electric and magnetic quantities is illustrated clearly. Specifically, we find that:

1. The presence of the magnetostrictive layer causes relatively large stress in the B/F/B sphere while the piezoelectric layer reduces the corresponding stress.
2. The fully coupled MEE sphere induces large values of electric displacement and magnetic induction in the innermost layer.
3. Unlike the majority of the MEE field variables, the components of radial stress have little dependence on stacking sequence.

These features would be valuable references when designing layered spherical structures made of MEE materials.

Acknowledgments

This work was supported by the National Natural Science Foundation of China (No. 11172273) and Bairen Project of Henan Province (China).

References

Abramovitz, M., Stegun, I.A. (Eds.), 1972. Handbook of Mathematical Functions with Formulas, Graphs, and Mathematical Tables. Dover, New York.
Chen, W.Q., Ding, H.J., 2001. Free vibration of multi-layered spherically isotropic hollow spheres. Int. J. Mech. Sci. 43, 667–680.
Chen, W.Q., Ding, H.J., Xu, R.Q., 2001. Three-dimensional static analysis of multi-layered piezoelectric hollow spheres via the state space method. Int. J. Solids Struct. 38, 4921–4936.
Chen, J.Y., Chen, H.L., Pan, E., 2007a. Modal analysis of magneto-electro-elastic plates using the state-vector approach. J. Sound Vib. 304, 722–734.
Chen, J.Y., Pan, E., Chen, H.L., 2007b. Wave propagation in magneto-electro-elastic multilayered plates. Int. J. Solids Struct. 44, 1073–1085.
Chen, J.Y., Heyliger, P.R., Pan, E., 2014. Free vibration of three-dimensional multilayered magneto-electro-elastic plates under combined clamped/free boundary conditions. J. Sound Vib. 333, 4017–4029.
Ding, H.J., Chen, W.Q., 1996. Natural frequencies of an elastic spherically isotropic hollow sphere submerged in a compressible fluid medium. J. Sound Vib. 192, 173–198.
Eerenstein, W., Mathur, N.D., Scott, J.F., 2006. Multiferroic and magnetoelectric materials. Nature 442, 759–765.
Heyliger, P., Wu, Y.C., 1999. Electroelastic fields in layered piezoelectric spheres. Int. J. Eng. Sci. 37, 143–161.
Kuo, H.Y., Pan, E., 2011. Effective magnetoelectric effect in multicoated circular fibrous multiferroic composites. J. Appl. Phys. 109, 104901.
Nan, C.W., Bichurin, M.I., Dong, S.X., Viehland, D., Srinivasan, G., 2008. Multiferroic magnetoelectric composites: historical perspective, status, and future directions. J. Appl. Phys. 103, 031101.
Pan, E., 2001. Exact solution for simply supported and multilayered magneto-electro-elastic plates. J. Appl. Mech. 68, 608–618.
Pan, E., Heyliger, P.R., 2002. Free vibrations of simply supported and multilayered magneto-elector-elastic plates. J. Sound Vib. 252, 429–442.

Ulitko, A.F., 1979. Method of special vector functions in three-dimensional elasticity. Naukova Dumka, Kiev, 264pp (in Russian)..

Wang, J.G., Chen, L.F., Fang, S.S., 2003. State vector approach to analysis of multilayered magneto-electro-elastic plates. Int. J. Solids Struct. 40, 1669–1680.

Watson, H.R., Singh, S.J., 1972. Static deformation of a multilayered sphere by internal sources. Geophys. J. R. Astron. Soc. 27, 1–14.

Xue, C.X., Pan, E., 2013. On the longitudinal wave along a functionally graded magneto-electro-elastic rod. Int. J. Eng. Sci. 62, 48–55.

Yu, J.G., Ding, J.C., Ma, Z.J., 2012. On dispersion relations of waves in multilayered magneto-electro-elastic plates. Appl. Math. Model. 36, 5780–5791.

Yu, J.G., Lefebvre, J.E., Zhang, C., 2014. Guided wave in multilayered piezoelectric–piezomagnetic bars with rectangular cross-sections. Compos. Struct. 116, 336–345.